

# Doping Dependent In-Plane and Cross-Plane Thermoelectric Performance of Thin n-Type Polymer P(NDI2OD-T2) Films

Regina M. Kluge, Nitin Saxena, Wei Chen, Volker Körstgens, Matthias Schwartzkopf, Qi Zhong, Stephan V. Roth, and Peter Müller-Buschbaum\*

Thermoelectric generators pose a promising approach in renewable energies as they can convert waste heat into electricity. In order to build high efficiency devices, suitable thermoelectric materials, both n- and p-type, are needed. Here, the n-type high-mobility polymer poly[N,N'-bis(2-octyldodecyl)naphthalene-1,4,5,8-bis(dicarboximide)-2,6-diyl]-alt-5,5'-(2,2'-bithiophene) (P(NDI2OD-T2)) is focused upon. Via solution doping with 4-(1,3-dimethyl-2,3-dihydro-1H-benzimidazol-2-yl)-N,N-diphenylaniline (N-DPBI), a maximum power factor of  $(1.84 \pm 0.13) \mu\text{W K}^{-2} \text{m}^{-1}$  is achieved in an in-plane geometry for 5 wt% dopant concentration. Additionally, UV-vis spectroscopy and grazing-incidence wide-angle X-ray scattering are applied to elucidate the mechanisms of the doping process and to explain the discrepancy in thermoelectric performance depending on the charge carriers being either transported in-plane or cross-plane. Morphological changes are found such that the crystallites, built-up by extended polymer chains interacting via lamellar and  $\pi$ - $\pi$  stacking, re-arrange from face- to edge-on orientation upon doping. At high doping concentrations, dopant molecules disturb the crystallinity of the polymer, hindering charge transport and leading to a decreased power factor at high dopant concentrations. These observations explain why an intermediate doping concentration of N-DPBI leads to an optimized thermoelectric performance of P(NDI2OD-T2) in an in-plane geometry as compared to the cross-plane case.


## 1. Introduction

Organic materials are emerging as potential candidates for thermoelectric applications as they combine relevant advantages such as low thermal conductivity, cost-effectiveness, environmental friendliness, solution processability, light weight, and mechanical flexibility. The latter properties make organic materials especially promising for wearable electronics as

their flexibility allows them to adapt to any curved surface such as human skin and, therefore, establish good thermal contact. To date, most organic materials being investigated are p-type,<sup>[1-5]</sup> while their n-type counterparts<sup>[6-10]</sup> do not show the same level of development and, thus, lead to comparatively lower power factors. The difficulty in finding stable and efficient n-type doping processes may originate from the small electron affinities of organic semiconductors as well as their high sensitivity toward oxygen and moisture.<sup>[11]</sup> Nonetheless, also high-performance n-type organic materials are needed in order to build an actual all-organic thermoelectric generator. Here, we investigate the high-mobility, air-stable n-type polymer poly[N,N'-bis(2-octyldodecyl)naphthalene-1,4,5,8-bis(dicarboximide)-2,6-diyl]-alt-5,5'-(2,2'-bithiophene) (P(NDI2OD-T2)).<sup>[12]</sup> In previous studies, different approaches were employed in order to improve the performance of P(NDI2OD-T2) in organic field-effect transistors, solar cells, and thermoelectric applications. In this regard,

annealing processes,<sup>[13-15]</sup> the choice of a suitable solvent,<sup>[16-18]</sup> chemical modifications,<sup>[19,20]</sup> and doping with different chemicals<sup>[6,7,21-24]</sup> were reported. Among these dopants, benzimidazole derivatives showed great success.<sup>[7,24]</sup> Therefore, we choose 4-(1,3-dimethyl-2,3-dihydro-1H-benzimidazol-2-yl)-N,N-diphenylaniline (N-DPBI) in order to dope P(NDI2OD-T2) in an easy solution-based process. In order to gain more detailed insights into the doping process, we performed UV-vis and

R. M. Kluge, Dr. N. Saxena, W. Chen, Dr. V. Körstgens, Prof. P. Müller-Buschbaum  
Physik Department  
Lehrstuhl für Funktionelle Materialien  
Technische Universität München  
James-Franck-Str. 1, Garching 85748, Germany  
E-mail: muellerb@ph.tum.de

 The ORCID identification number(s) for the author(s) of this article can be found under <https://doi.org/10.1002/adfm.202003092>.

© 2020 The Authors. Published by WILEY-VCH Verlag GmbH & Co. KGaA, Weinheim. This is an open access article under the terms of the Creative Commons Attribution License, which permits use, distribution and reproduction in any medium, provided the original work is properly cited.

DOI: 10.1002/adfm.202003092

Dr. M. Schwartzkopf, Prof. S. V. Roth  
DESY  
Notkestraße 85, Hamburg 22607, Germany

Prof. Q. Zhong  
Key Laboratory of Advanced Textile Materials and Manufacturing Technology  
Ministry of Education  
Zhejiang Sci-Tech University  
Hangzhou 310018, China

Prof. S. V. Roth  
KTH  
Department of Fibre and Polymer Technology  
Teknikringen 56-58, Stockholm SE-100 44, Sweden  
Prof. P. Müller-Buschbaum  
Heinz Maier-Leibnitz-Zentrum  
Lichtenbergstr. 1, Garching 85748, Germany

grazing-incidence wide-angle X-ray scattering (GIWAXS) measurements on the thin films with different dopant concentrations. During these investigations, it turns out that the dopant is introducing additional charges to the polymer chains with increasing dopant concentration while the morphology of the system is highly anisotropic. Therefore, we investigate the thermoelectric performance, that is, the power factor, in two different charge transport directions: parallel (in-plane) and perpendicular (cross-plane) to the substrate. In this regard, we obtain a maximum power factor of  $(1.84 \pm 0.13) \mu\text{W K}^{-2} \text{m}^{-1}$ , which can compete with previously reported thermoelectric performances of other solution-processable n-type polymers<sup>[6–8]</sup> and hence renders the polymer P(NDI2OD-T2) interesting for being used in thermoelectric generators.

## 2. Results and Discussion

In the present study, the optical, morphological, and thermoelectric properties of P(NDI2OD-T2) thin films upon doping with concentrations between 0 and 40 wt% N-DPBI are investigated. Details on the sample preparation, a simple solution-based process, can be found in the Experimental Section.

### 2.1. Optical Properties

In terms of optical properties, a color change of the samples with increasing dopant concentrations is directly visible by eye as shown in the photograph (Figure 1b). Since this color change indicates an interaction between polymer and dopant, conducting a UV-vis measurement as a first step is straightforward.

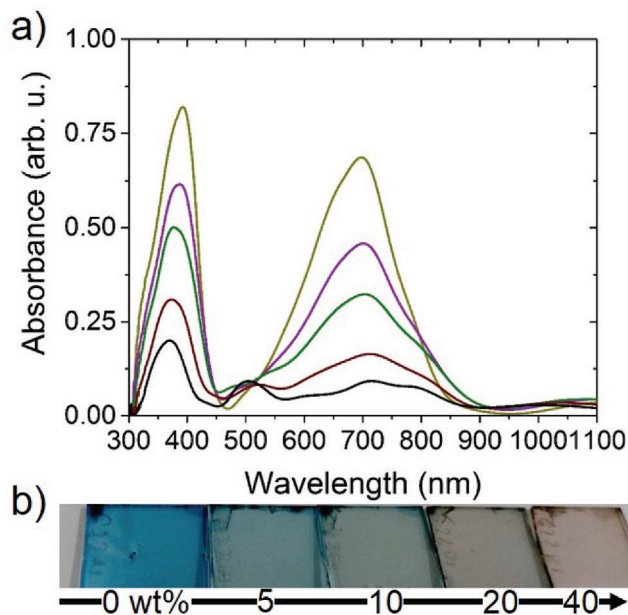


**Figure 1.** a) UV-vis spectra of P(NDI2OD-T2) in its undoped state (dark yellow) and with 5 wt% (purple), 10 wt% (green), 20 wt% (maroon), and 40 wt% (black) N-DPBI doping. b) Photograph showing the color change of the thin film samples upon doping with increasing N-DPBI concentration from left to right.

It is known that also the spectrum of pure thiophene nanoparticles undergoes changes upon doping, such that a new feature arises at around 770 nm.<sup>[25,26]</sup> Focusing to begin with only on the spectrum of pure P(NDI2OD-T2), the dark yellow curve in Figure 1a, a high-energy peak centered at 380 nm corresponding to the  $\pi$ - $\pi$  transition and a broad low-energy band centered at 700 nm assigned to the charge-transfer (CT) transition can be distinguished.<sup>[17]</sup> A CT transition in donor-acceptor co-polymers like P(NDI2OD-T2) occurs when a significant amount of charge carriers is redistributed from the donor to the acceptor moiety, that is, from the thiophenes to the naphthalene diimide conjugated core. Upon doping, both of these peaks are decreasing in intensity while two new bands arise at approximately 500 and 800 nm which can be assigned to the emergence of negative polarons.<sup>[27]</sup> Simultaneously, the  $\pi$ - $\pi$  transition peak undergoes a blue-shift upon doping. This is uncommon for doped polymers as their UV-vis spectra usually show a redshift upon doping due to the occurrence of polaronic states in the band gap which lowers the band gap energy.<sup>[8,28]</sup> Such a deviation may indicate that it is in fact not only the formation of polaronic bands but also a morphology change occurring in doped P(NDI2OD-T2). These morphology changes are discussed below in more detail. The reported trends in the UV-vis spectrum of doped P(NDI2OD-T2) are in accordance with previous studies employing solvent and vapor doping with different materials.<sup>[6,29]</sup> The appearance of polaronic species in the UV-vis spectrum upon doping already indicates a charge transfer from dopant to the polymer and therefore successful doping. The reaction between dopant and polymer is believed to take place via a hydride transfer (Figure S1, Supporting Information).<sup>[7,30]</sup>

Upon air exposure, the initial color of the doped films dulls toward the blue shade of pristine P(NDI2OD-T2) indicating a certain change of the doped polymer chains that will be further investigated using UV-vis. The color and spectrum of the pristine polymer show no changes upon air exposure confirming that the pure polymer is stable in air as reported previously.<sup>[12,21]</sup> However, air exposure has an effect on all doped samples and is most significant for the 40 wt% doping concentration shown in Figure 2a. With time the polaronic bands are decreasing while the  $\pi$ - $\pi$  and CT peaks are increasing in intensity which seems to be inverse to what is happening when doping the pristine polymer film. However, during this development, the spectra of the doped samples do not fully approach the spectrum of undoped P(NDI2OD-T2). The decrease of the polaronic bands indicates a loss of charge of the polymer chains which is most probably caused by oxidation. Besides the stability of the system in air, its stability toward temperature needs to be tested as the material is investigated for thermoelectric applications. Therefore, temperature-dependent UV-vis measurements are carried out. Hereby, the sample holder is heated step-wise from room temperature to 100 °C. After a short equilibration time, a UV-vis measurement is performed in the same manner as at room temperature. In order to distinguish changes caused by heat from changes caused by air exposure, a reference sample is measured simultaneously at room temperature. It turns out that the influence of temperature on the degradation of the films is most tremendous when the doping concentration is high. Therefore, the temperature-dependent measurement for the 40 wt%-sample is shown in Figure 2c,d whereas Figure 2a,b

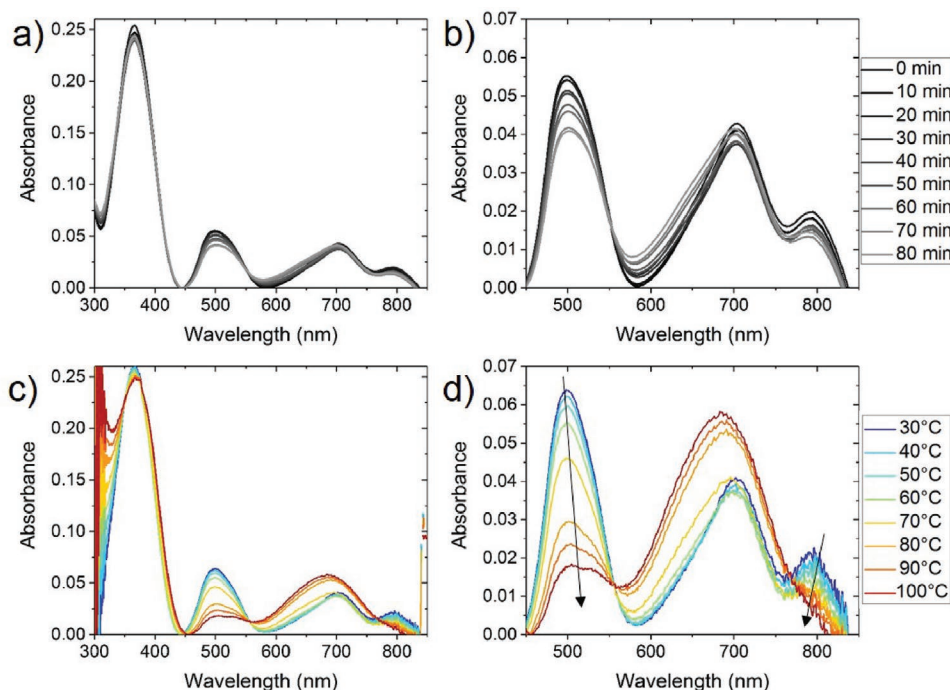


**Figure 2.** a) UV-vis spectra of a 40 wt%-doped P(NDI2OD-T2) film in dependence on air exposure time. The measurements are conducted at room temperature. b) Enlargement of (a) in the wavelength range of 450–850 nm. c) Temperature-dependent UV-vis spectra of a 40 wt%-doped sample. d) Enlargement of (c) in the wavelength range of 450–850 nm. Both measurements are carried out simultaneously in intervals of 10 min. In the temperature-dependent measurement, the temperature is ramped from room temperature to 100 °C in 10 °C steps while the reference measurement is conducted at room temperature. In comparison, a steep decrease in the polaronic bands at approximately 500 and 800 nm can be observed at temperatures higher than 80 °C as indicated by the arrows in figure (d).

depicts the corresponding reference measurement. We observed that the polaronic peak at 500 nm steeply decreases between 70 and 80 °C in comparison to the reference. This leads to the conclusion that temperatures above 70 °C facilitate degradation of highly doped samples (40 wt%) probably because the oxidation reaction is accelerated at higher temperatures. The development of the UV-vis spectra of samples with lower dopant concentrations (0, 5, 10, and 20 wt%) with air exposure time and temperature are given in Figure S2, Supporting Information. From these measurements we deduce that the degradation is not occurring at temperatures up to 100 °C as long as low dopant concentrations is used. We assume that the samples are stable below this temperature and temperature can be reversibly changed.

In summary, we used UV-vis spectroscopy as a tool to qualitatively measure the degree of doping through the appearance of additional polaronic bands and moreover to make a statement about degradation mechanisms.

## 2.2. Film Morphology

The appearance of polaronic bands in the UV-vis spectra is a first hint that the polymer is electronically doped by the dopant. However, besides charge carrier concentration also the morphology is crucial for charge transport. Therefore, GIWAXS is applied to probe the morphology of the polymer as a function of dopant concentration. The GIWAXS data of pure P(NDI2OD-T2) shown in Figure 3b is in good accordance with

the literature.<sup>[29,31]</sup> We employ the literature model, in which extended polymer chains orient with the backbone preferentially parallel to the substrate<sup>[31,32]</sup> and form lamellae.<sup>[17,33–35]</sup> Within these lamellae, the molecules are oriented in a face-on manner.<sup>[17,31]</sup> In a system similar to ours, the polymer chains within the lamellae interact with each other via segregated  $\pi$ - $\pi$  stacking, meaning that only donor-donor and acceptor-acceptor  $\pi$ - $\pi$  stacking occurs.<sup>[36]</sup> Concerning electron mobility, the crystallinity along the  $\pi$ - $\pi$  stacks is crucial as charges are supposed to be transported along them. In this regard, non-conjugated side chains are believed to act as hopping barriers and also lamellar ordering seems to have less impact on charge transport.<sup>[6,36,37]</sup> On larger length scales, flat plate-like crystalline domains are built up from polymer chains interacting via lamellar and  $\pi$ - $\pi$  stacking.<sup>[31,36,38]</sup> With increasing film thickness, more and more of these crystallites lay on top of each other being slightly misaligned with respect to the crystallites underneath. Nonetheless, the orientation of these crystallites shows a distinct face-on orientation.<sup>[15,31]</sup> This nano-scale organization is observed in the range of nm to  $\mu$ m in spin-coated films.<sup>[35]</sup>

Upon doping, the GIWAXS data in Figure 3 show different trends in the lamellar (h00) and  $\pi$ - $\pi$  (00l) stacking peaks. For the in-plane lamellar stacking, one can observe a decrease in intensity until the (200)<sub>ip</sub> peak completely vanishes at 40 wt%. Simultaneously, new out-of-plane peaks arise at similar q-values which we therefore assign to an out-of-plane lamellar stacking. While the (100)<sub>op</sub> peak already appears at

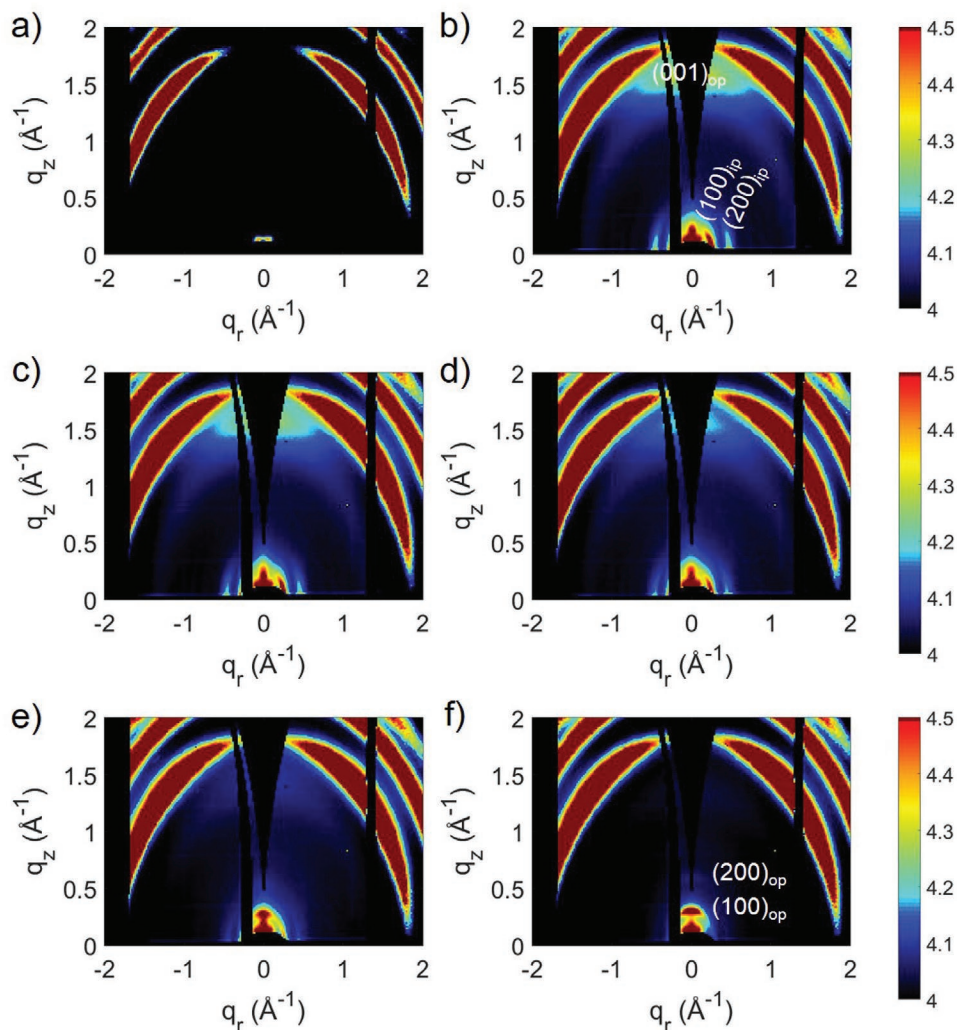


**Figure 3.** GIWAXS data of the a) FTO substrate, b) pristine P(NDI2OD-T2), and c–f) doped P(NDI2OD-T2) with concentrations of 5, 10, 20, and 40 wt%, respectively, each on FTO substrates. The peaks are denoted with (h00) for lamellar and (00l) for  $\pi$ - $\pi$  stacking.

5 wt%, the  $(200)_{op}$  reflection only becomes visible at 20 wt%. In order to examine the behavior of the lamellar stacking peaks further, sector integrals are executed horizontally and vertically. The in-plane lamellar stacking is probed by performing a horizontal cake cut and integrating over angles from  $70^\circ$  to  $80^\circ$  with respect to the specular plane. Likewise, vertical cake cuts from  $-15^\circ$  to  $15^\circ$  are performed to probe the out-of-plane lamellar stacking. All peaks are fitted by Gaussian functions. The results are shown in Figure 4a,b. It is clearly visible that the peaks in the horizontal respectively vertical cuts lose respectively gain intensity confirming what has been explained before. In order to show the spatial development of the first lamellar peak in a more detailed way, a tube integral is performed around the  $(100)$  peak integrating over all  $q$ -values from  $0.2$  to  $0.3 \text{ \AA}^{-1}$ . In Figure 4c the result is shown. The face-on-to-edge-on intensity ratio is calculated by dividing the amplitude of the  $(100)_{op}$  peak by the amplitude of the  $(100)_{ip}$  and is plotted in Figure 4e. This value points out that the orientation of the crystallites changes from preferentially face-on to a preferential edge-on configuration. Another trend visible in the GIWAXS data in Figure 3

is that the  $\pi$ - $\pi$  stacking peak  $(100)_{op}$  loses intensity and finally vanishes with increasing doping concentration. The occurrence of a new in-plane  $\pi$ - $\pi$  stacking reflex cannot be observed. This can be confirmed by performing a tube-cut around the center of the  $\pi$ - $\pi$  stacking peak integrating over  $q$ -values from  $1.58$  to  $1.61 \text{ \AA}^{-1}$ . The decrease in intensity of the peaks can be clearly seen in Figure 4d.

Summarizing, we come up with a morphological model shown in Figure 4f. Upon doping, the crystallites, built from lamellar and  $\pi$ - $\pi$  stacking, rotate their orientation from face-on to edge-on. At the same time, the direction of the  $\pi$ - $\pi$ -stacking and thus also the direction of charge transport additionally changes from out-of-plane to in-plane direction. However, at the same time, the  $\pi$ - $\pi$  stacking gets less pronounced. Bearing this in mind, the results indicate that the crystallites do not only reorient but also the order within these crystals gets weaker. Most likely the dopant molecules are incorporated within the crystallites and therefore disturb the ordering of the polymer chains.

Comparing these findings to literature is challenging as there are not many studies on the morphology of doped

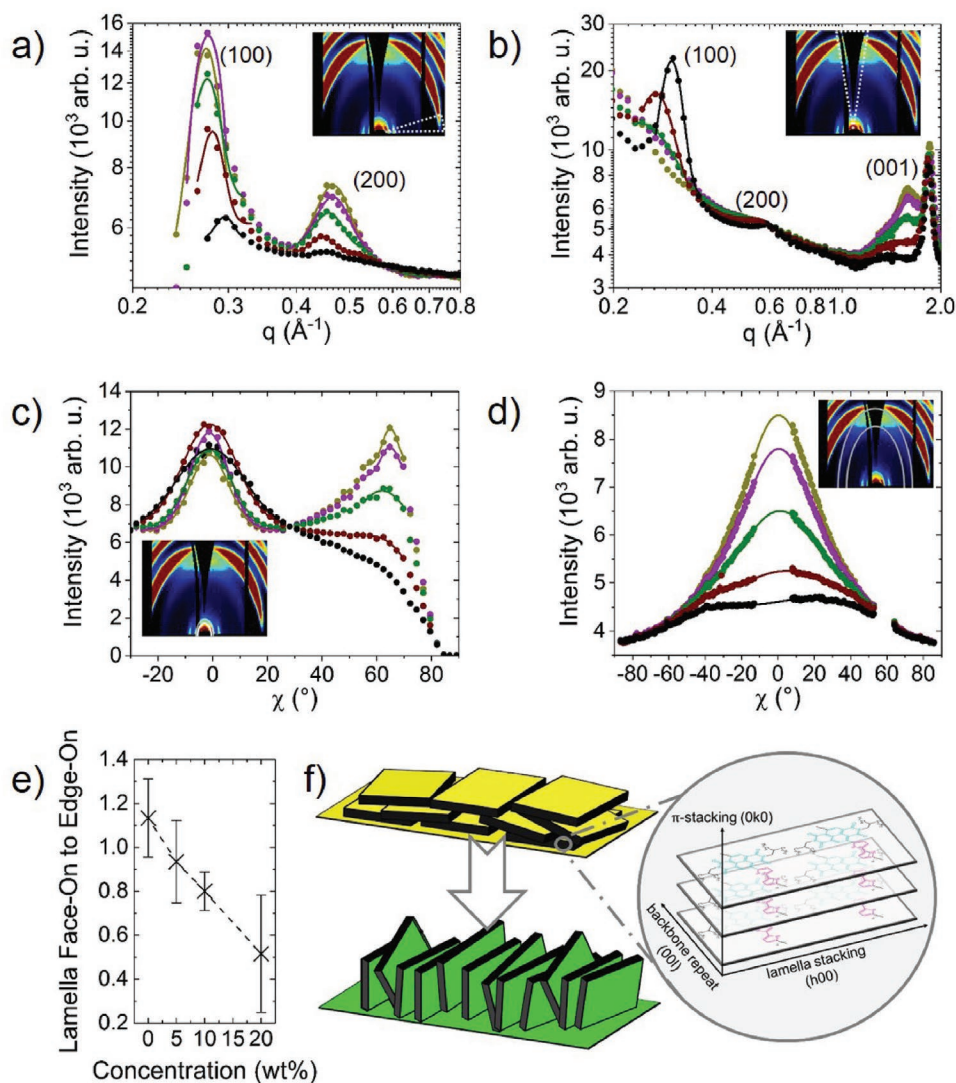


**Figure 4.** a) Vertical and b) horizontal sector integrals to extract first and second order in-plane respectively out-of-plane lamellar (100) and (200) Bragg peaks as well as the first out-of-plane  $\pi$ - $\pi$  peak. Tube integrals centered on c) the first lamellar stacking peak and d) the  $\pi$ - $\pi$  stacking peak as a function of doping concentration with 0 wt% (dark yellow), 5 wt% (purple), 10 wt% (green), 20 wt% (maroon), and 40 wt% (black). e) Face-on to edge-on intensity ratio calculated from the lamellar tube integrals. f) Morphological model in which the crystallites turn their orientation from edge-on to face-on since the lamellar stacking within the crystallites changes direction from in-plane to out-of-plane. Moreover, the  $\pi$ - $\pi$  stacking gets less prominent at high dopant concentrations due to dopant molecules being increasingly incorporated into the crystallites thereby disturbing their order.

P(NDI2OD-T2) in general and GIWAXS studies in particular. Wang et al. report for their reference system P(NDI2OD-T2) that the in-plane lamellar reflections decrease while the out-of-plane  $\pi$ - $\pi$  stacking smooths out.<sup>[6]</sup> Liu et al. report that upon doping with cobaltocene the in-plane lamellar stacking increases and subsequently decreases upon further addition of dopant.<sup>[21]</sup> Both observations are in accordance with ours. Moreover, Naab et al. state for (2-Cyc-DMBI)<sub>2</sub>-doped P(NDI2OD-T2) that the in-plane lamellar and backbone reflections decrease in intensity and the out-of-plane  $\pi$ - $\pi$  stacking peak is smoothed out to a halo centered at  $1.55 \text{ \AA}^{-1}$ . Moreover, they find the appearance of a new in-plane peak at  $1.88 \text{ \AA}^{-1}$  and assign it to  $\pi$ - $\pi$  stacking.<sup>[29]</sup> While the trends concerning the lamellar stacking are in accordance with our findings, the appearance of a new in-plane  $\pi$ - $\pi$  peak is not observed in the

present study. This can either be because there is none as our system slightly differs because of another derivative of the doping material or the new peak may be covered by the FTO substrate contribution.

In addition, we also conduct this study on glass (Figure S4, Supporting Information) where we do not observe the rise of an in-plane  $\pi$ - $\pi$  stacking peak whereas all other findings are in accordance with the ones for the polymer thin films on an FTO substrate reported here.

### 2.3. Thermoelectric Properties

Having discussed the possible influences on charge carrier concentration and morphology of P(NDI2OD-T2) upon reacting

with the dopant N-DPBI, which are both crucial for charge transport, we are now able to not only report but also explain its thermoelectric properties. Motivated by the anisotropic morphology of the system, two different sample geometries are established in order to probe the charge transport in-plane, that is, parallel to the substrate and cross-plane, that is, perpendicular to the substrate. More details on the samples' geometry and preparation can be found in the Experimental Section. The measurement techniques are introduced in the same place as well as in previous publications.<sup>[39]</sup>

### 2.3.1. In-Plane Geometry

In the beginning, the "traditional" in-plane geometry is investigated. The electrical resistance in dependence on temperature shown in **Figure 5a** is measured with a home-made set-up. When looking only at the pristine polymer (dark yellow curve), the tremendous fluctuations of the resistance at lower temperatures are attributed to the insulating character of the undoped polymer, which prevents a reasonable measurement. Nonetheless, the overall drop in resistance of the doped films with respect to the pure polymer indicates successful doping with N-DPBI. The observation of successful doping is in good agreement with the UV-vis measurements that show charge transfer of the dopant to the polymer and the formation of polaronic bands. Paying attention to the shape of the resistance curves of the doped polymers, a decrease in resistance with temperature can be observed first. This trend is in accordance with the expected semiconducting behavior of the polymer. However,

above 80 °C the trend inverses and the resistance increases again. This resistance increase at elevated temperatures is in line with the observations indicating a facilitated oxidation process in the same temperature range (UV-vis Spectroscopy, **Figure 2**). In order to prevent this acceleration of the degradation process, the maximum temperature for all subsequent measurements is lowered to 70 °C. From resistance and sample geometry, the electrical conductivity is extracted exemplarily for 30 and 70 °C and is shown in **Figure 5b**. For both temperatures, the conductivity first increases and subsequently decreases with a maximum of  $(10.8 \pm 0.6) \times 10^{-3} \text{ S cm}^{-1}$  at 10 wt% doping concentration. The same trend in conductivity has also been observed in other studies.<sup>[6,7,29]</sup>

Bearing in mind the results of the UV-vis and GIWAXS studies, it is possible to explain this trend. At low doping concentration, charge carriers are introduced to the polymer, increasing the conductivity. At the same time, the crystallites re-orient to a more edge-on configuration. In this orientation the  $\pi$ - $\pi$  stacks are parallel to the charge transport, that is, in-plane, further improving charge transport and subsequently the conductivity. At even higher dopant concentrations, the UV-vis study reveals that more and more charge carriers are introduced to the polymer. In addition, the re-orientation of the molecules gets even stronger however at the expense of the  $\pi$ - $\pi$  stacking and order within the crystallites which decreases. This is most likely due to the dopant molecules being incorporated within the crystallites and disturbing the ordering of the polymer chains. Due to the loss of order the transport of the increased number of charge carriers is hindered and the conductivity again decreases upon high doping concentrations.

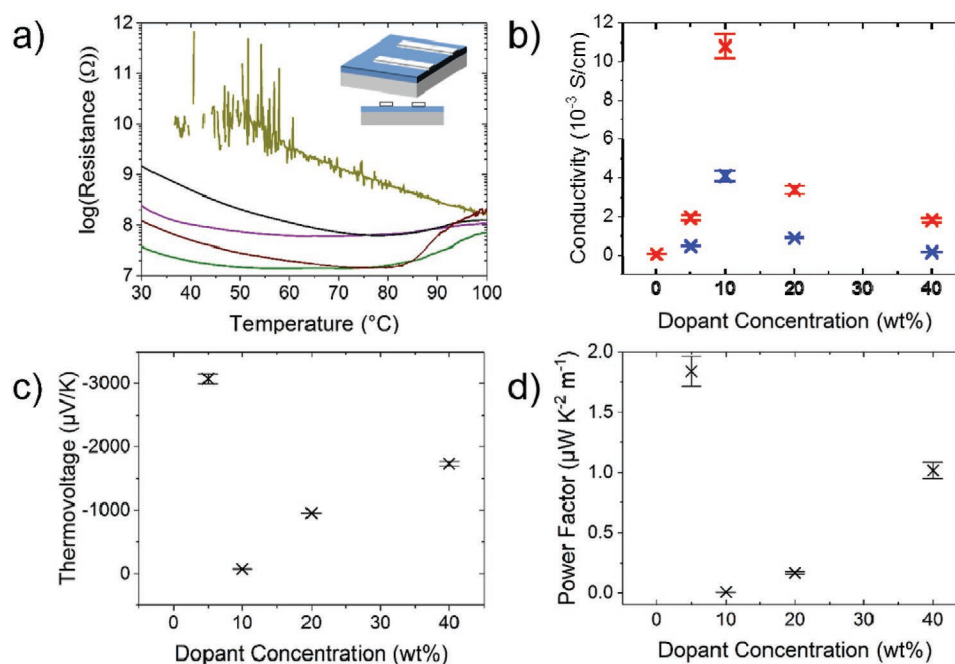


**Figure 5.** Thermoelectric properties measured in in-plane geometry. a) Resistance curves of undoped P(NDI2OD-T2) (dark yellow) and with 5 wt% (purple), 10 wt% (green), 20 wt% (maroon), and 40 wt% (black) N-DPBI. The inset depicts the samples' geometry in top and side view consisting of a glass substrate (grey), the thin film (blue), and two aluminum electrodes (light grey). b) Conductivities extracted for 30 °C (blue symbols) and 70 °C (red symbols). c) Thermovoltage measured at 70 °C mean temperature. d) Power factor  $\text{PF} = S^2\sigma$  calculated from thermovoltage  $S$  and conductivity  $\sigma$  at 70 °C.

In addition to the conductivity a second thermoelectric quantity, the Seebeck coefficient, is measured by applying a temperature gradient of 20 °C at a mean temperature of 70 °C. Note that the Seebeck coefficient of the pristine sample was not accessible in the measurement which we ascribe to its low intrinsic conductivity. In comparison to the electrical conductivity, it shows the inverse trend with respect to the dopant concentration. Thereby, a maximum Seebeck coefficient of  $-(3074 \pm 77) \mu\text{V K}^{-1}$  is obtained at 5 wt%. This may be explained by the fact that these two properties are inversely proportional to the charge carrier concentration. The inverse trends for conductivity and thermovoltage with respect to doping concentration have also been observed for other polymers.<sup>[10,40–42]</sup>

The power factor at 70 °C is calculated from the conductivity  $\sigma$  and thermovoltage  $S$  values via  $S^2\sigma$ . It results in a maximum power factor of  $(1.84 \pm 0.13) \mu\text{W K}^{-2} \text{m}^{-1}$  for 5 wt% dopant concentration at elevated temperatures. The discrepancy between the optimum value of doping concentration for conductivity and power factor comes from the fact that the power factor is governed by the Seebeck coefficient. The obtained power factor is higher than previously reported values for this very system<sup>[7]</sup> and it is only one order of magnitude lower than for most p-type polymers thereby approaching their performance.

### 2.3.2. Cross-Plane Geometry

Subsequently, the cross-plane properties of the system are investigated. As for the in-plane measurement, the resistance decreases upon doping proven by the resistance curves as a

function of temperature shown in **Figure 6a**. But in contrast to the in-plane measurement where the resistance varies through several orders of magnitude, the change in cross-plane resistance stays within one order of magnitude. Resistance values are on the order of  $10^4 \Omega$  which is significantly smaller than the in-plane resistances which are of the order of  $10^7 \Omega$  and higher. Furthermore, the cross-plane resistance of the pristine sample could be measured also in contrast to the in-plane measurements. Remarkably, the resistance curves exhibit increasing fluctuations with increasing doping concentration. These fluctuations in the resistance are again attributed to a decreasing conductivity value and therefore deteriorated contact to the measurement tips.

The extracted conductivity values are on the order of  $10^{-9} \text{ S cm}^{-1}$  and therefore around six orders of magnitude smaller than those for the in-plane conductivity. The reason why the conductivity is so low even though the resistance values are lower than for the in-plane sample geometry is that the distance the charge carriers have to overcome in order to reach from one electrode to the other enters into the equation used to calculate the conductivity via the resistance. The formulas can be found in the Experimental Section. In the in-plane case, this distance is on the order of centimeters while for the cross-plane case the distance, namely, the film thickness is on the order of nanometers and therefore orders of magnitude smaller. Using again the information gained from UV-vis and GIWAXS, the trends in cross-plane conductivity can be explained. Since the orientation of the molecules in the pristine state is preferentially face-on, this favors the charge transport perpendicular to the substrate along the  $\pi$ - $\pi$

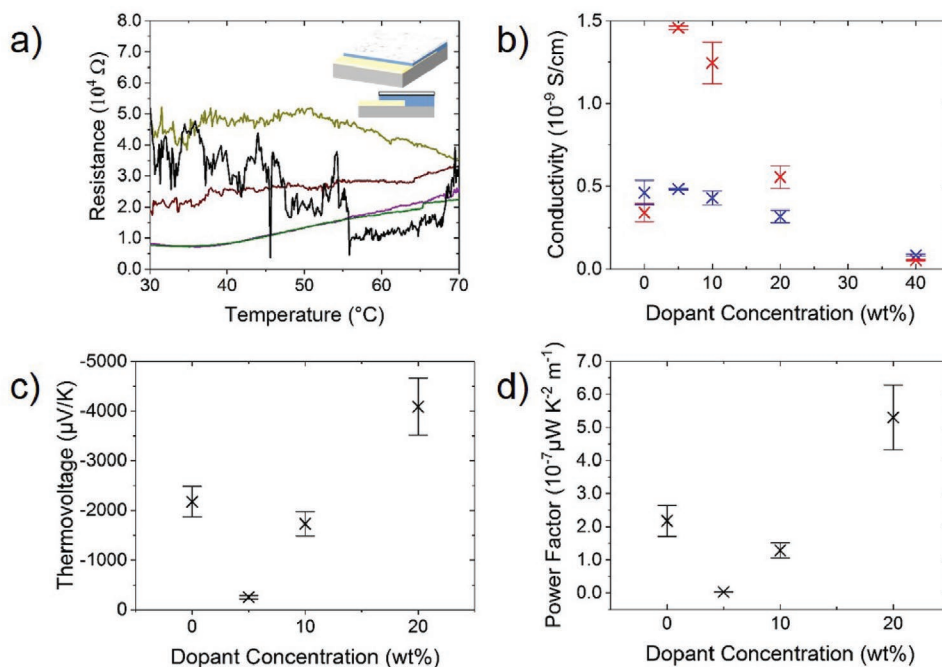


**Figure 6.** Thermoelectric properties measured in cross-plane geometry. a) Resistance curves of undoped P(NDI2OD-T2) (dark yellow) and with 5 wt% (purple), 10 wt% (green), 20 wt% (maroon), and 40 wt% (black) N-DPBI. The inset depicts the samples' geometry in top and side view consisting of an FTO-coated (yellow) glass (grey) substrate, the thin film (blue), and an aluminum electrode (light grey). b) Electrical conductivities extracted for 30 °C (blue symbols) and 70 °C (red symbols). c) Thermovoltage measured at 70 °C mean temperature. d) Power factor  $\text{PF} = S^2\sigma$  calculated from thermovoltage  $S$  and conductivity  $\sigma$  at 70 °C.

stacking direction. Upon intermediate doping of 5 to 10 wt% charge carriers are introduced and the conductivity is therefore increased. However, at the same time, the crystallites rearrange from face- to edge-on. This change is unfavorable for cross-plane transport as the direction of the  $\pi$ - $\pi$  stacks is altered from former out-of-plane to in-plane. Additionally, the dopant molecules start to interrupt the polymer's order. This change in morphology cannot be compensated by the introduction of additional charges. Therefore, at further doping, the conductivity value decreases. Furthermore, the thermovoltage shows an opposing trend to the electrical conductivity, as is also found for the in-plane geometry. It is not possible to obtain a stable thermovoltage for a dopant concentration of 40 wt%, which may be due to the very low conductivity and a bad contact between electrodes and measurement tips, as mentioned above. The experiment results in an overall maximum power factor of  $(5.31 \pm 0.98) \times 10^{-8} \mu\text{W K}^{-2} \text{m}^{-1}$  for 20 wt% dopant concentration and therefore almost eight orders of magnitude smaller than for the in-plane charge transport. This large difference in in- and cross-plane efficiency can be explained by the anisotropic morphology of the system.

### 3. Conclusions

In the present study, the thermoelectric properties of the n-type polymer P(NDI2OD-T2) have been investigated. While the polymer is electrically insulating in its pristine state, doping with the small molecule N-DPBI increases the electrical conductivity as well as the thermoelectric properties, that is, the power factor, drastically. It is believed that the doping process takes place by a hydride transfer. In this regard, UV-vis spectroscopy is used as a simple yet powerful tool to confirm the introduction of additional charges to the polymer chain. The measurement technique can also be applied to detect degradation mechanisms in air or in combination with air and elevated temperature. In order to observe morphological changes within the material upon doping, GIWAXS experiments are carried out. They revealed that upon doping, the orientation of the flat plate-like crystallites, made up from lamellar and  $\pi$ - $\pi$  stacking interactions between extended polymer chains, changes from mainly face-on to edge-on. With this change, also the direction of the  $\pi$ - $\pi$  stacks, along which the charges are transported, changes from out-of-plane to in-plane. However, toward higher doping concentrations the order within these crystallites decreases. This trend can be explained by an increasing number of dopant molecules incorporated in the crystallites. In order to link the anisotropic morphology of the system with its thermoelectric properties, we probe charge transport in two geometries: in-plane and cross-plane. Thereby we observe that the in-plane performance of a maximum power factor of  $(1.84 \pm 0.13) \mu\text{W K}^{-2} \text{m}^{-1}$  is several orders of magnitude higher than for the cross-plane case. This discrepancy in performance can be explained by taking into account the reported anisotropic morphology of the doped thin films. Upon doping, charge carrier concentration increases and the molecules re-orient from a face-on to an edge-on configuration. The latter includes the direction of the  $\pi$ - $\pi$  stacks to

change from out-of-plane to in-plane facilitating charge transport in in-plane while hindering charge transport in out-of-plane direction, thus, explaining why in-plane transport is favorable over cross-plane transport.

### 4. Experimental Section

**Sample Preparation:** P(NDI2OD-T2) and N-DPBI were purchased from 1-MATERIAL Inc. and Sigma-Aldrich Chemie GmbH, respectively, and used as received. The choice of materials as well as parts of the sample preparation were based on the work of Schlitz and coworkers.<sup>[7]</sup> For the in-plane measurements, glass was used as a substrate and thoroughly cleaned in a diluted piranha solution (DI-H<sub>2</sub>O: H<sub>2</sub>O<sub>2</sub> [30%]: H<sub>2</sub>SO<sub>4</sub> [95–97%] in a ratio of 9:14:33). For the cross-plane measurements, FTO substrates were used and cleaned by subsequent immersion in the detergent Alconox, ethanol, acetone, and isopropanol. In order to prevent oxidation of the active layer, all following steps including solution preparation, spin-coating, and annealing were carried out in nitrogen atmosphere. Polymer and dopant were separately dissolved in 1,2-dichlorobenzene (99%, Sigma-Aldrich) at a concentration of 10 mg mL<sup>-1</sup>, each. Only for the cross-plane samples the concentration of the polymer was enhanced to 20 mg mL<sup>-1</sup> to increase the film's thickness. Both polymer and dopant solution were then stirred separately at 80 °C for 30 min. The polymer was filtered through a 0.45  $\mu\text{m}$  PTFE filter and subsequently mixed with the dopant in concentrations between 0 and 40 wt%. The mixture was then stirred again at 80 °C for 2 h and applied to the substrate via spin-coating. As electrodes two aluminum stripes of  $(2 \times 15) \text{ mm}^2$  area were evaporated on top of the film in a distance of 10 mm. In cross-plane geometry, the doped polymer film was sandwiched between an FTO bottom and an aluminum top electrode with an active area of  $(11 \times 25) \text{ mm}^2$ .

**UV-Vis Spectroscopy:** The measurements were carried out using a Lambda35 UV-vis spectrometer (PerkinElmer Inc.) from 300 to 1100 nm with an accuracy of  $\pm 0.1 \text{ nm}$ .

**GIWAXS Study:** Measurements on FTO substrates took place at the P03/MiNaXS beamline of the PETRA III storage ring at the Deutsches Elektronen-Synchrotron in Hamburg.<sup>[43]</sup> Synchrotron radiation of 0.0957 nm wavelength impinged the sample at an angle of 0.2° at a sample detector distance of 0.150 m using a Pilatus 300k (Dectris Ltd.) detector. In order to avoid beam damage, measurement times of 10 s were chosen. The obtained detector images were interpreted and analyzed using the MATLAB-based software GIXSGUI.<sup>[44]</sup>

**Thermoelectric Measurements:** The thermoelectric measurements were carried out using a home-made set-up. Temperature-dependent resistance measurements were performed by placing the sample on a heating stage, ramping-up the temperature of the sample in a controlled way. Meanwhile, two measurement tips were placed on both electrodes, a two-point probe measurement was performed by applying a constant voltage. The conductivity was extracted from the resistance  $R$  via Equations (1) and (2) including geometric considerations like the film thickness  $t$ , the distance  $d$ , and the length  $l$  of the electrodes in in-plane geometry and the active electrode area  $A$  in cross-plane geometry.

$$\sigma_{in} = \frac{d}{Rl} \quad (1)$$

$$\sigma_{cross} = \frac{t}{RA} \quad (2)$$

For the determination of the in-plane Seebeck coefficient, the sample was placed across two copper blocks out of which one was heated using a heating cartridge and the other one cooled by the flow of water. After some equilibration time achieving a constant temperature gradient, the voltage and the temperature difference between both electrodes was measured and the Seebeck coefficient was calculated. Likewise, for the cross-plane Seebeck coefficient, the sample was placed on a hotplate



establishing a temperature gradient between the bottom and top electrodes.

## Supporting Information

Supporting Information is available from the Wiley Online Library or from the author.

## Acknowledgements

The authors acknowledge funding from Deutsche Forschungsgemeinschaft (DFG, German Research Foundation) under Germany's Excellence Strategy—EXC 2089/1—390776260 (e-conversion) and via International Research Training Group 2022 Alberta/Technical University of Munich International Graduate School for Environmentally Responsible Functional Materials (ATUMS) as well as from the Center for NanoScience (CeNS). W.C. acknowledges the China Scholarship Council (CSC) funding. GIWAXS experiments were carried out at the light source PETRA III at DESY, a member of the Helmholtz Association (HGF).

## Conflict of Interest

The authors declare no conflict of interest.

## Keywords

crystal orientation, doping, n-type, power factor, thermoelectric polymers

Received: April 7, 2020  
Revised: April 24, 2020  
Published online: May 25, 2020

- [1] C. Cho, B. Stevens, J.-H. Hsu, R. Bureau, D. A. Hagen, O. Regev, C. Yu, J. C. Grunlan, *Adv. Mater.* **2015**, *27*, 2996.
- [2] S. N. Patel, M. L. Chabiny, *J. Appl. Polym. Sci.* **2017**, *134*, 44403.
- [3] G.-H. Kim, L. Shao, K. Zhang, K. P. Pipe, *Nat. Mater.* **2013**, *12*, 719.
- [4] O. Bubnova, Z. U. Khan, A. Malti, S. Braun, M. Fahlman, M. Berggren, X. Crispin, *Nat. Mater.* **2011**, *10*, 429.
- [5] N. Saxena, J. Keilhofer, A. K. Maurya, G. Fortunato, J. Overbeck, P. Müller-Buschbaum, *ACS Appl. Energy Mater.* **2018**, *1*, 336.
- [6] S. Wang, H. Sun, U. Ail, M. Vagin, P. O. A. Persson, J. W. Andreasen, W. Thiel, M. Berggren, X. Crispin, D. Fazzi, S. Fabiano, *Adv. Mater.* **2016**, *28*, 10764.
- [7] R. A. Schlitz, F. G. Brunetti, A. M. Gludell, P. L. Miller, M. A. Brady, C. J. Takacs, C. J. Hawker, M. L. Chabiny, *Adv. Mater.* **2014**, *26*, 2825.
- [8] B. Russ, A. Gludell, J. J. Urban, M. L. Chabiny, R. A. Segalman, *Nat. Rev. Mater.* **2016**, *1*, 16050.
- [9] Y. Sun, P. Sheng, C. Di, F. Jiao, W. Xu, D. Qiu, D. Zhu, *Adv. Mater.* **2012**, *24*, 932.
- [10] K. Shi, F. Zhang, C.-A. Di, T.-W. Yan, Y. Zou, X. Zhou, D. Zhu, J.-Y. Wang, J. Pei, *J. Am. Chem. Soc.* **2015**, *137*, 6979.
- [11] H. T. Nicolai, M. Kuik, G. A. H. Wetzelaer, B. de Boer, C. Campbell, C. Risko, J. L. Bredas, P. W. M. Blom, *Nat. Mater.* **2012**, *11*, 882.
- [12] H. Yan, Z. Chen, Y. Zheng, C. Newman, J. R. Quinn, F. Dotz, M. Kastler, A. Facchetti, *Nature* **2009**, *457*, 679.
- [13] S. Fabiano, H. Yoshida, Z. Chen, A. Facchetti, M. A. Loi, *ACS Appl. Mater. Interfaces* **2013**, *5*, 4417.
- [14] V. D'Innocenzo, A. Luzio, A. Petrozza, D. Fazzi, M. Caironi, *Adv. Funct. Mater.* **2014**, *24*, 5584.
- [15] J. Rivnay, R. Steyrleuthner, L. H. Jimison, A. Casadei, Z. Chen, M. F. Toney, A. Facchetti, D. Neher, A. Salleo, *Macromolecules* **2011**, *44*, 5246.
- [16] A. Luzio, L. Criante, V. D'Innocenzo, M. Caironi, *Sci. Rep.* **2013**, *3*, 3425.
- [17] R. Steyrleuthner, M. Schubert, I. Howard, B. Klaumunzer, K. Schilling, Z. Chen, P. Saalfrank, F. Laquai, A. Facchetti, D. Neher, *J. Am. Chem. Soc.* **2012**, *134*, 18303.
- [18] M. Schubert, D. Dolfen, J. Frisch, S. Roland, R. Steyrleuthner, B. Stiller, Z. Chen, U. Scherf, N. Koch, A. Facchetti, D. Neher, *Adv. Energy Mater.* **2012**, *2*, 369.
- [19] Z. Li, J. D. A. Lin, H. Phan, A. Sharenko, C. M. Proctor, P. Zalar, Z. Chen, A. Facchetti, T.-Q. Nguyen, *Adv. Funct. Mater.* **2014**, *24*, 6989.
- [20] J. W. Jung, J. W. Jo, C.-C. Chueh, F. Liu, W. H. Jo, T. P. Russell, A. K.-Y. Jen, *Adv. Mater.* **2015**, *27*, 3310.
- [21] C. Liu, J. Jang, Y. Xu, H.-J. Kim, D. Khim, W.-T. Park, Y.-Y. Noh, J.-J. Kim, *Adv. Funct. Mater.* **2015**, *25*, 758.
- [22] Y. Qi, S. K. Mohapatra, S. Bok Kim, S. Barlow, S. R. Marder, A. Kahn, *Appl. Phys. Lett.* **2012**, *100*, 083305.
- [23] A. Higgins, S. K. Mohapatra, S. Barlow, S. R. Marder, A. Kahn, *Appl. Phys. Lett.* **2015**, *106*, 163301.
- [24] B. D. Naab, S. Zhang, K. Vandewal, A. Salleo, S. Barlow, S. R. Marder, Z. Bao, *Adv. Mater.* **2014**, *26*, 4268.
- [25] X. G. Li, M. R. Huang, *Chem. - Eur. J.* **2009**, *15*, 6446.
- [26] X. G. Li, Q. K. Meng, M. R. Huang, *J. Phys. Chem. B* **2009**, *113*, 9718.
- [27] M. Caironi, M. Bird, D. Fazzi, Z. Chen, R. di Pietro, C. Newman, A. Facchetti, H. Sirringhaus, *Adv. Funct. Mater.* **2011**, *21*, 3371.
- [28] J. L. Bredas, G. B. Street, *Acc. Chem. Res.* **1985**, *18*, 309.
- [29] B. D. Naab, X. Gu, T. Kurosawa, J. W. F. To, A. Salleo, Z. Bao, *Adv. Electron. Mater.* **2016**, *2*, 1600004.
- [30] P. Wei, J. H. Oh, G. Dong, Z. Bao, *J. Am. Chem. Soc.* **2010**, *132*, 8852.
- [31] J. Rivnay, M. F. Toney, Y. Zheng, I. V. Kauvar, Z. Chen, V. Wagner, A. Facchetti, A. Salleo, *Adv. Mater.* **2010**, *22*, 4359.
- [32] E. Giussani, D. Fazzi, L. Brambilla, M. Caironi, C. Castiglioni, *Macromolecules* **2013**, *46*, 2658.
- [33] T. Schuettfort, L. Thomsen, C. R. McNeill, *J. Am. Chem. Soc.* **2013**, *135*, 1092.
- [34] V. Lemaire, L. Muccioli, C. Zannoni, D. Beljonne, R. Lazzaroni, J. Cornil, Y. Olivier, *Macromolecules* **2013**, *46*, 8171.
- [35] C. J. Takacs, N. D. Treat, S. Krämer, Z. Chen, A. Facchetti, M. L. Chabiny, A. J. Heeger, *Nano Lett.* **2013**, *13*, 2522.
- [36] R. Steyrleuthner, R. di Pietro, B. A. Collins, F. Polzer, S. Himmelberger, M. Schubert, Z. Chen, S. Zhang, A. Salleo, H. Ade, A. Facchetti, D. Neher, *J. Am. Chem. Soc.* **2014**, *136*, 4245.
- [37] J. Rivnay, S. C. B. Mannsfeld, C. E. Miller, A. Salleo, M. F. Toney, *Chem. Rev.* **2012**, *112*, 5488.
- [38] A. M. Anton, R. Steyrleuthner, W. Kossack, D. Neher, F. Kremer, *Macromolecules* **2016**, *49*, 1798.
- [39] N. Saxena, M. Čorić, A. Greppmair, J. Wernecke, M. Pflüger, M. Krumrey, M. S. Brandt, E. M. Herzig, P. Müller-Buschbaum, *Adv. Electron. Mater.* **2017**, *3*, 1700181.
- [40] W. Ma, K. Shi, Y. Wu, Z.-Y. Lu, H.-Y. Liu, J.-Y. Wang, J. Pei, *ACS Appl. Mater. Interfaces* **2016**, *8*, 24737.
- [41] X. Zhao, D. Madan, Y. Cheng, J. Zhou, H. Li, S. M. Thon, A. E. Bragg, M. E. DeCoster, P. E. Hopkins, H. E. Katz, *Adv. Mater.* **2017**, *29*, 1606928.
- [42] J. Wüsten, K. Potje-Kamloth, *J. Phys. D: Appl. Phys.* **2008**, *41*, 135113.
- [43] A. Buffet, A. Rothkirch, R. Döhrmann, V. Köstgens, M. M. Abul Kashem, J. Perlich, G. Herzog, M. Schwartzkopf, R. Gehrke, P. Müller-Buschbaum, S. V. Roth, *J. Synchrotron Radiat.* **2012**, *19*, 647.
- [44] Z. Jiang, *J. Appl. Crystallogr.* **2015**, *48*, 917.